ELSEVIER

Journal of Nuclear Materials 280 (2000) 86–98

journal of nuclear materials

www.elsevier.nl/locate/jnucmat

Analysis of fission gas release and gaseous swelling in UO_2 fuel under the effect of external restraint

Yang-Hyun Koo *, Byung-Ho Lee, Dong-Seong Sohn

Future Fuel Development, Korea Atomic Energy Research Institute, 150 Duckjin-dong, Yusong-gu, Daejon 305-303, South Korea

Received 21 December 1998; accepted 7 February 2000

Abstract

To analyze fission gas release and gaseous swelling in UO_2 fuel, a model has been developed that can be used under both steady-state and transient operating conditions up to high burnup. With emphasis on the effect of external restraint stress on the behavior of gas bubbles at grain boundaries, the gaseous swelling due to grain edge bubbles, which affects gas release rate through the formation of release tunnels at grain edge, is described. Gas release rate at the grain edge is assumed to be proportional to both the fraction of grain edge bubbles interlinked to open space of fuel and the rate of gas atoms arriving at the grain edge bubbles. The model was compared with the data obtained from commercial reactors, Risφ-III Project, isothermal irradiation and post-irradiation annealing experiments. It is shown that the model predicts well the fractional fission gas release as well as the radial distribution of Xe gas across fuel pellet under various operating conditions. This suggests that the present model can be used for the analysis of fission gas release at high burnup fuel where strong external restraint stress may develop due to pellet cladding interaction.

PACS: 28.41.B

1. Introduction

When extending current LWR fuel burnup, fission gas release is generally considered to be a potential design limitation factor because of its impact on cladding integrity through increased internal pressure. In addition, the mechanical restraint caused by pellet cladding mechanical interaction (PCMI) together with high internal pressure, which acts as an external restraint, affects the gaseous swelling at grain boundaries that is related to the formation of release path and hence fission gas release. Zimmermann [1] performed an irradiation test under isothermal annealing conditions, which showed that a compressive load significantly reduced gas bubble swelling. Kogai et al. [2,3] revealed that fission gas release can be different depending on the extent of PCMI, that is, external restraint. After the extensive investigation of the radial fission gas distribution obtained by XRF and EPMA for the transient-tested fuels, Walker et al. [4] concluded that fuel temperature and mechanical restraint are of equal importance in determining the extent of gas bubble interlinkage at the grain boundary and the level of gas release during power transients. Turnbull and Tucker [5,6] showed that compressive stress in UO_2 fuel inhibits the development of grain face bubbles and beyond a certain level, it may prevent the formation of grain edge bubbles. Kashibe and Une [7] performed an experiment, which confirms that the bubble growth in unirradiated UO_2 fuel is strongly influenced by an external restraint even at the high annealing temperatures from 1600°C to 1800°C.

Once PCMI develops and hence external restraint exerts a compressive force on the fuel during steady-state operation, the amount of gas atoms that is retained in the grain boundaries would be increased while delaying and reducing gas release depending on the magnitude of the restraint. Under transient operating conditions when gas release occurs through the microcracks created by change in thermal stress, the gas

* Corresponding author. Tel.: +82-42 868 8728; fax: +82-42 864 1089.

E-mail address: yhkoo@nanum.kaeri.re.kr (Y.-H. Koo).

0022-3115/00/$ - see front matter
PII: S0022-3115(00)00034-9

release would be also enhanced by the external restraint if it had existed during the previous steady-state operation because it would have increased the amount of gas atoms in the grain boundaries. Furthermore, since the gaseous swelling, which has an important role in determining the degree of PCMI in high burnup fuel where pellet-to-cladding gap is narrow or already closed due to the swelling of solid fission products and cladding creepdown, would be governed by the external restraint, cladding integrity is also closely related to the external restraint. Therefore, the effect of external restraint should be considered so that the gas release and gaseous swelling in high burnup fuel, where strong PCMI might exist, can be predicted appropriately during both the steady-state and transient conditions.

In the present paper, a fission gas release model is developed considering the effect of external restraint on the behavior of gas bubbles in the grain boundaries. In the model, gaseous swelling induced by the grain face and grain edge bubbles is treated as a function of external stress, which is the sum of rod internal pressure and external restraint caused by PCMI. Using the assumption that UO_2 grain face is composed of 14 identical circular faces [8], a grain edge bubble in this geometry is represented by a triangulated tube around the circumference of the grain face. Then a concept of the formation of release tunnels at grain edges is introduced in such a way that the degree of the formation of release paths is proportional to the gas bubble swelling at the grain edges. In addition, by taking into account the effect of fuel temperature on gaseous swelling, the model treats the dependence of the formation of release paths on fuel temperature for the same number of gas atoms retained in the grain boundaries. This implies that the model can predict the generally observed enhanced gas release at high burnup fuel through larger gaseous swelling, that is through more release tunnels, which is caused by increased fuel temperature resulting from the degradation of thermal conductivity with burnup for the same power. The model has been incorporated into a fuel performance analysis code COSMOS [9] and evaluated using irradiation data obtained from a wide range of operating conditions.

2. Model development

2.1. Intragranular behavior

Under normal operating conditions where gas atom migration is the dominant mechanism by which gas reaches the grain boundary [10–12], two rate equations that describe the number of gas atoms in a dynamic solution and intragranular bubbles, and the number of gas atoms released to the grain boundary are expressed by

$$\frac{dc}{dt} = \beta - \frac{dm}{dt} - \frac{dg_b}{dt}, \tag{1}$$

$$\frac{dm}{dt} = g_i c - b_i m, \tag{2}$$

where c is the number of gas atoms in a dynamic solution (atoms/m^3), β the gas atom production rate which is $0.3F$ (atoms/m^3 s), F the fission density (fissions/m^3 s), m the number of gas atoms in intragranular bubbles (atoms/m^3), g_b the number of gas atoms released to the grain boundary (atoms/m^3), and b_i is the resolution probability from intragranular bubbles (1/s) [13].

In solving the two equations, g_i, which is defined as the probability per second that gas atoms in a dynamic solution in the matrix would be captured by a bubble of radius ρ_i, is given by $4\pi DC_B\rho_i$ [13,14]. In addition, the number of gas atoms released to the grain boundary up to time t, g_b, is described as follows [13]:

$$g_b = f_c\beta t + f_A\left(c - c_\lambda^{max}\right), \tag{3}$$

where

$$f_c = \begin{cases} 4(w/\pi)^{1/2} - 1.5w & \text{for } f_c < 0.57, \\ 1 - 0.0662[1 - 0.93\exp(-\pi^2 w)]/w & \text{for } f_c \geqslant 0.57, \end{cases} \tag{4}$$

$$f_A = \begin{cases} 6(w/\pi)^{1/2} - 3w & \text{for } f_A < 1/\pi^2, \\ 1 - 6\exp(-\pi^2 w)/\pi^2 & \text{for } f_A \geqslant 1/\pi^2. \end{cases} \tag{5}$$

Here $w = Dt/a^2$, a is the grain radius (m), and D is the diffusion coefficient of fission gas in the matrix (m^2/s) [14]. c_λ^{max} is the gas atom concentration at resolution depth from grain boundary,

$$c_\lambda^{max} = b_f\lambda N_f^{max}/2D \text{ (atoms/m}^3\text{)} \tag{6}$$

where b_f is the resolution probability from grain face bubbles (1/s), λ the resolution layer depth from grain face (10^{-8} m), and N_f^{max} is the maximum number of gas atoms stored at the grain face (atoms/m^2) which is $C_f m_f$ (see Section 2.2 for C_f and m_f).

Eqs. (1)–(6) can be solved numerically to obtain the number of fission gas atoms retained both in the matrix and the intragranular bubbles, and the gas number released to the grain boundary as a function of irradiation conditions and time.

2.2. Grain face behavior

To treat the behavior of grain face bubbles, it is assumed that a fixed concentration of grain face bubbles are allowed to grow according to the arrival rate of gas atoms to the grain face. Once the grain face bubbles cover a certain fraction of grain face area, all the gas

atoms reaching the grain face are assumed to be released to the grain edge. Furthermore, it is also assumed that the gas atoms arriving at the grain face are equally distributed among the fixed concentration of bubbles. After the saturation of grain face, all the gas atoms arriving at the grain face are considered to be released to the grain edge. Therefore, after grain face saturation, m_f remains unchanged just maintaining the saturation values required for the specific time-step during which fuel temperature is almost constant. Then under these circumstances, the rate equation that accounts for the number of gas atoms on the grain face is described as follows before the grain face is saturated:

$$\frac{d}{dt}(C_f m_f) = 2\left\{1 - \left(\frac{\Delta S}{S}\right)_e\right\}\frac{a}{3}\frac{dg_b}{dt}, \tag{7}$$

where C_f is the concentration of grain face bubbles (bubbles/m^2), which is $1.928 \times 10^3 \exp[3.312\times 10^4/T(K)]$ (at low temperatures, C_f is given an upper limiting value of 10^{14} [15]), m_f is the number of gas atoms in a bubble of radius of curvature ρ_f (atoms/bubble), and $(\Delta S/S)_e$ is the fraction of grain edge area occupied by tunnels (see Section 2.3).

Since the fraction of grain face f_b covered by gas bubbles is expressed by $C_f\pi\rho_f^2\sin^2\theta$, the maximum radius of curvature ρ_f^{max} of a grain face bubble required for grain face saturation is

$$\rho_f^{max} = \left(f_b^{max}/C_f\pi\sin^2\theta\right)^{1/2}, \tag{8}$$

where f_b^{max} is the maximum coverage of grain face by gas bubbles and θ is the semi-dihedral angle defining the shape of a gas bubble. The generally accepted value for θ is 50°. Therefore, if ρ_f is less than ρ_f^{max}, no release from the grain face to grain edge occurs except for direct release from the matrix to grain edge. After grain face saturation, however, all the gas atoms arriving at the grain face are assumed to be released to the grain edge. There are several values for the maximum coverage of grain face by bubbles f_b^{max} depending on models or observations: 0.25 [13], 0.50 [16] or 0.70 [8].

It is assumed that the gas pressure in the grain face bubble is always balanced by the sum of lattice surface tension and local hydrostatic stress, that is, the bubbles are always in equilibrium. By applying the ideal gas law, the number of gas atoms m_f in a bubble of radius of curvature ρ_f required for mechanical stability is given as

$$m_f = \frac{PV_{gf}}{kT} = \frac{4\pi\rho_f^3}{3kT}f_f(\theta)\left(\frac{2\gamma}{\rho_f} + \sigma_r\right), \tag{9}$$

where k is the Boltzmann constant, $f_f(\theta)$, which is the geometric factor relating the volume of a grain face bubble to that of a sphere, is $1 - 3\cos\theta/2 + \cos\theta^3/2$ and σ_r is the external restraint stress on fuel pellet. If the fuel pellet is in compression, then σ_r is taken to be positive.

In the case that there is no PCMI or σ_r is negligibly small and hence $2\gamma/\sigma_r\rho_f$ is much larger than 1, ρ_f is derived as follows from Eq. (9):

$$\rho_f = \left(\frac{3kTm_f}{8\pi\gamma f_f(\theta)}\right)^{1/2}. \tag{10}$$

On the other hand, if PCMI takes place and the substantial contact pressure develops such that $2\gamma/\sigma_r\rho_f$ is much smaller than 1, then ρ_f is given as

$$\rho_f = \left(\frac{3kTm_f}{4\pi f_f(\theta)\sigma_r}\right)^{1/3}. \tag{11}$$

The maximum difference between the approximate solution of Eq. (10) or Eq. (11) and the exact solution for the condition of $2\gamma/\sigma_r\rho_f$ being equal to one is 21%. However, as $2\gamma/\sigma_r\rho_f$ deviates from one, the difference decreases rapidly thereby showing that Eq. (10) or Eq. (11) can be used to calculate ρ_f instead of a very complex exact solution.

The fractional volume swelling due to the grain face bubbles, normalized to the unit volume of the grain matrix, is computed by

$$\left(\frac{\Delta V}{V}\right)_f = \frac{1}{2}\frac{4\pi a^2 C_f}{4\pi a^3/3}\left(\frac{4}{3}\pi\rho_f^3 f_f(\theta)\right) = \frac{1}{a}2\pi C_f f_f(\theta)\rho_f^3, \tag{12}$$

where the factor 1/2 is necessary because a grain face bubble is shared by two neighboring grains.

Eqs. (7) and (10)–(12) are solved numerically to obtain the number of gas atoms contained in a grain face bubble, the radius of curvature of a grain face bubble, and the swelling due to grain face bubbles.

2.3. Grain edge behavior

To treat the gas release from the grain face to grain edge and gaseous swelling, a UO_2 grain surface is assumed to be composed of 14 identical circular faces [8]. Then a grain edge bubble in this geometry, which is represented by a triangulated tube around the circumference of the grain face (Fig. 1), is shared by three neighboring grains and is bounded by three identical circular faces. The gas atoms collected here are assumed to be distributed evenly so that the circular edges form a torus where the fission gas atoms are stored. Furthermore, the release rate from the grain edge to open surface is assumed to be proportional to both the instantaneous fission gas inventory at the grain edge and the fraction of grain edge bubbles interlinked to the open surface. Before the grain face is saturated, only direct release from the matrix to the grain edge exists.

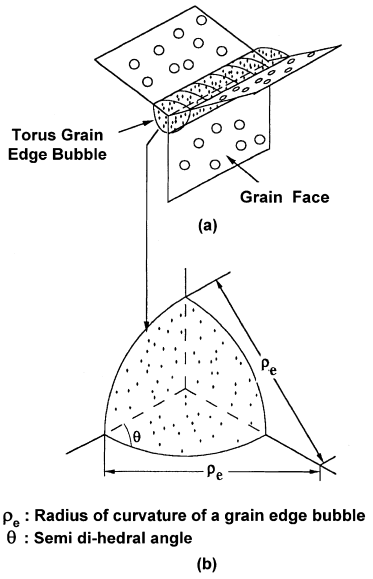

Fig. 1. Schematic diagram of a torus grain edge bubble: (a) side view; (b) cross-sectional view.

Then the rate equation describing the concentration of fission gas atoms in a grain edge bubble is expressed as follows before the grain face is saturated:

$$2\pi r_{\mathrm{gf}}\frac{\mathrm{d}c_{\mathrm{e}}}{\mathrm{d}t}=3(1-f)\pi r_{\mathrm{gf}}^2\left(\frac{\Delta S}{S}\right)_{\mathrm{e}}\frac{a}{3}\frac{\mathrm{d}g_{\mathrm{b}}}{\mathrm{d}t}, \tag{13}$$

where c_{e} is the gas atom concentration in a bubble along grain edge (atoms/m), f the fraction of grain edge bubble interlinked to open surfaces (see Section 2.4), r_{gf} the radius of curvature of a circular grain face which is $0.5557a$ [13], and $(\Delta S/S)_{\mathrm{e}}$ is $1.29(\rho_e/a)-0.6041(\rho_{\mathrm{e}}/a)^2$ [13].

After grain face saturation, according to the assumption of Section 2.2 that all the gas atoms arriving at the grain boundary are released to the grain edge, the rate equation for the grain edge concentration is given as

$$2\pi r_{\mathrm{gf}}\frac{\mathrm{d}c_{\mathrm{e}}}{\mathrm{d}t}=3(1-f)\pi r_{\mathrm{gf}}^2\frac{a}{3}\frac{\mathrm{d}g_{\mathrm{b}}}{\mathrm{d}t}. \tag{14}$$

The number of gas atoms in a grain edge bubble, which is a circular torus in the present model, is calculated by

$$m_{\mathrm{e}}=2\pi r_{\mathrm{gf}}c_{\mathrm{e}}. \tag{15}$$

As in the case of a grain face bubble, the bubble gas pressure is assumed to be always balanced by the sum of lattice surface tension and the local hydrostatic stress. Then the number of gas atoms m_{e} required for mechanical stability in a triangulated grain edge bubble with the radius of curvature ρ_{e} is calculated from

$$m_{\mathrm{e}}=\frac{V_{\mathrm{e}}}{kT}\left(\frac{2\gamma}{\rho_{\mathrm{e}}}+\sigma_{\mathrm{r}}\right), \tag{16}$$

where

$$V_e=2\pi r_{\mathrm{gf}}\{\pi\rho_e^2 f_t(\theta)\},$$

$$f_t(\theta)=\frac{3}{\pi}\left\{\theta-\frac{\pi}{6}-2\cos\theta\,\sin(\theta-\frac{\pi}{6})/\sqrt{3}\right\},$$

(see [13]). In the case that there is no PCMI and hence σ_{r} is zero, ρ_{e} is derived as follows from Eqs. (15) and (16):

$$\rho_{\mathrm{e}}=\frac{kTc_{\mathrm{e}}}{2\pi\gamma f_t(\theta)}. \tag{17}$$

On the other hand, if PCMI takes place and the contact pressure develops, ρ_{e} is given by

$$\rho_{\mathrm{e}}=-\frac{\gamma}{\sigma_{\mathrm{r}}}+\sqrt{\left(\frac{\gamma}{\sigma_{\mathrm{r}}}\right)^2+\left(\frac{kTc_{\mathrm{e}}}{\pi f_t(\theta)\sigma_{\mathrm{r}}}\right)}. \tag{18}$$

The fractional volume swelling of the grain edge bubbles, normalized to the unit volume of the grain matrix, is calculated by

$$\left(\frac{\Delta V}{V}\right)_{\mathrm{e}}=\frac{14}{3}\frac{1}{4\pi a^3/3}2\pi r_{\mathrm{gf}}\{\pi\rho_{\mathrm{e}}^2 f_t(\theta)\}=\frac{7\pi}{a^3}r_{\mathrm{gf}}f_t(\theta)\rho_{\mathrm{e}}^2, \tag{19}$$

where the factor 1/3 is introduced since a grain edge bubble is shared by three neighboring grains and the factor 14 is multiplied because there are 14 circular faces per grain.

Eqs. (13), (14) and (17)–(19) are solved numerically to obtain the number of gas atoms contained in a grain edge bubble, the radius of curvature of a grain edge bubble, and the swelling due to grain edge bubbles.

2.4. Interlinkage at grain edge

Release pathways at grain edges are generally considered to be achieved suddenly at the moment when grain edge swelling reaches some preassigned value, for example, 5% [17], 7% [18] or 8% [19]. This approach, however, would rule out the possibility that gas release might take place even before the grain edge swelling reaches some threshold value. According to the percolation theory [20], networks such as grain edge tunnels have non-zero probability of being open at any instant of time. Hence, a long-range interlinkage among grain edge tunnels would be established at gaseous swelling less than the above-mentioned critical values at which all tunnels are suddenly interlinked to the fuel open space.

Based on this argument and the experimental results [21,22] that a linear relation exists between the degree of fuel swelling and the level of local release, it is assumed

that the fraction of grain edge bubbles interlinked to fuel open space f is proportional to the grain edge swelling as follows:

$$f = \frac{(\Delta V/V)_e}{(\Delta V/V)_e^{max}}, \tag{20}$$

where the upper limiting value of f is one. A similar approach was used by Sontheimer et al. [23] but their interlinkage factor was calculated using the integrated flux of gas atoms to the grain boundary. In addition, once the grain edge tunnels are developed, they are assumed to be stable during a time-step where fuel temperature is constant. This means that another f is developed in the next time-step corresponding to its temperature even if the number of the gas atoms retained in the grain edge remains unchanged. If the maximum grain edge swelling is achieved, all gas atoms that reach the grain edges would be released to fuel outside.

2.5. Fission gas release

2.5.1. Release via interlinked tunnel

The amount of fission gas released to the open space of fuel pellet through interlinked grain edge tunnels should be calculated by considering whether gas bubbles saturates the grain face or not because this determines the fission gas inventory at the grain edge available for release. Before the grain face is saturated, the gas release rate R_e is

$$R_e = \frac{1}{3} 14 f 3\pi r_{gf}^2 \left(\frac{\Delta S}{S}\right)_e \frac{a}{3} \frac{dg_b}{dt}, \tag{21}$$

where the factor 1/3 is introduced since a grain edge bubble is shared by three neighboring grains and the factor 14 is multiplied because there are 14 circular faces per grain.

After the saturation of grain face, all gas atoms released to the grain boundary would migrate to the grain edge thereby giving the gas release rate through the interlinked grain edge tunnel as follows:

$$R_e = \frac{1}{3} 14 f 3\pi r_{gf}^2 \frac{a}{3} \frac{dg_b}{dt}. \tag{22}$$

2.5.2. Release due to grain growth

Notley and Hastings [24] suggested that grain growth in enriched UO_2 can be described by the following equation:

$$(2a_i)^{2.5} - (2a_{i-1})^{2.5} = 1.7 \times 10^3 \Delta t \exp(-Q/RT), \tag{23}$$

where a_i is the grain radius after time Δt (μm), a_{i-1} the starting grain radius (μm), Δt the time interval (s), Q the activation energy which is 2.3×10^5 (J/mol), and R is the gas constant which is 8.314 (J/K mol).

The additional release rate of fission gas from the matrix to the grain boundary by grain growth N_{gg} is

$$N_{gg} = \frac{4}{3}\pi\left(a_i^3 - a_{i-1}^3\right)(c+m)/\Delta t. \tag{24}$$

It is assumed that the gas atoms released by grain growth are evenly distributed among the 14 grain edges. Then the increasing rate of fission gas concentration at each grain edge N_{ge} due to grain growth is

$$N_{ge} = \frac{N_{gg}}{14} = \frac{2\pi}{21\Delta t}\left(a_i^3 - a_{i-1}^3\right)(c+m). \tag{25}$$

If N_{ge} is assumed to be distributed uniformly along the length of toroid, the increase in concentration of gas atoms along the grain edge Δc_e is

$$\Delta c_e = \frac{N_{ge}}{2\pi r_{gf}} = \frac{1}{21 r_{gf}\Delta t}\left(a_i^3 - a_{i-1}^3\right)(c+m). \tag{26}$$

Consequently, if grain growth occurs at high temperature, the increased grain edge concentration calculated by Eq. (26) should be added to Eq. (13) or Eq. (14) to get the total grain edge concentration.

2.5.3. Release due to recoil and knock-out

At low temperatures, only the fission gases that are formed very close to an external surface can escape by recoil and knock-out. These release mechanisms, which are independent of both temperature and temperature gradient, affect only the outer layer of the fuel (within about 10 μm of the surface). The release rate per unit fuel volume due to recoil and knock-out R_v [25] is given as

$$R_v = \frac{yF}{4}\left(S_g\mu_g + 2S_t\mu_u^{ko}\right), \tag{27}$$

where y is the fission yield of stable fission products (0.3), F the fission density (fissions/m^3 s), S_g the geometrical surface area of the fuel (m^2), S_t the total surface area of the fuel (m^2), μ_g the range of the fission fragment in the fuel (10 μm), and μ_u^{ko} the range of higher order uranium knock-on in UO_2 (50 Å). If the number of grains per unit fuel volume is denoted as n_g, the release rate per grain R_d is R_v/n_g.

A fuel pellet can be divided into two regions depending on its temperature distribution [26]: (a) an inner plastic region with a temperature higher than 1400°C and (b) an outer region with a temperature below 1400°C and containing a number of radial cracks through which gas release can occur. Furthermore, Oguma [27] and Wood et al. [28] have shown that the number of pellet cracks increases almost linearly with fuel linear power and the number of radial fuel cracks is about one-half of the linear power (in kW/m). Based on these two observations, once the linear power and pellet dimensions are given, the total pellet surface area

available for gas release by recoil and knock-out can be calculated.

2.5.4. Release due to power transient

The gas release components given in Eqs. (21) and (22) apply only to the conditions where power remains constant or changes slowly versus time. There are many experimental findings showing that the burst of gas release exists during rapid power increase or decrease due to the microcracking of fuel pellets induced by change in thermal stress [29,30].

An empirical transient gas release model [29] is slightly modified to analyze gas release under power transient conditions. Once the conditions given below are satisfied, the entire gas inventory at grain boundaries is assumed to be released instantaneously. When linear power increases from q_1 to q_2, burst release occurs as a result of microcracking if $q_2 - q_1 > 30$ W/cm, $q_2 > 250$ W/cm, and $T_2 > T_g$. The burnup-dependent temperature threshold T_g is defined as $T_g = 1500(1 - \mathrm{BU}/80)$, where T_g is the fuel temperature in degree centigrade and BU is the burnup in MWd/kgU. Here q values are the linear powers in an axial segment considered and T_g values are the radial ring temperatures. In the case of power decrease from q_1 to q_2, burst release takes place through microcracking if $q_1 - q_2 > 30$ W/cm, $q_1 > 250$ W/cm, and $T_1 > T_g$. As shown in Table 2, the empirical gas release model, including the temperature threshold T_g, can be applied at least to a burnup of 44.5 MWd/kgU.

The number of gas atoms released from a grain by this mechanism is designated as N_{tr}. In the model, the gas inventory available for release during the power change is the sum of those at the grain face and grain edge.

2.5.5. Total release

The total number of gas atoms released to fuel free volume N_{tot} from a grain during time interval Δt is

$$N_{tot} = (R_e + R_d)\,\Delta t + N_{tr}. \tag{28}$$

3. Comparison with experimental data

The main physical parameters affecting gas release in the present model are the maximum grain edge swelling $(\Delta V/V)_e^{max}$, the maximum grain face area covered by gas bubbles f_b^{max}, and the intergranular re-solution probability b_f. For the present model, the maximum grain edge swelling at which release paths are completed is given as 0.07 [18]. The maximum fraction of grain face covered with bubbles f_b^{max} is assumed to be 0.50 [16,31]. Finally, the intergranular resolution probability b_f is taken to be 10^{-5} [32].

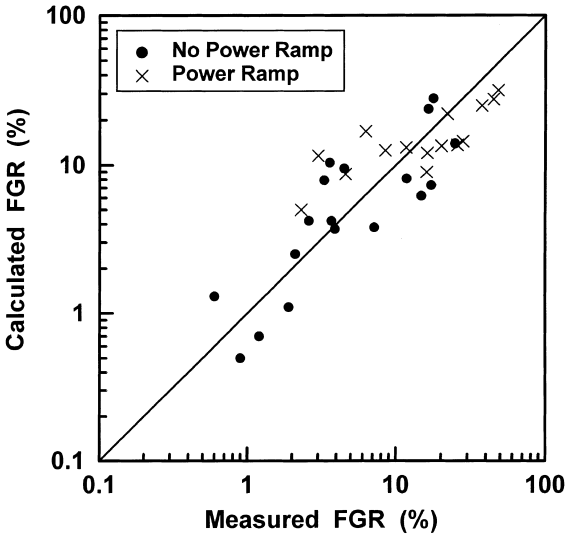

Fig. 2. Comparison of calculated and measured fission gas release for both power ramped and non-power ramped fuel rods.

To evaluate the model, it has been incorporated into a fuel performance analysis code COSMOS [9]. A comparison was made for a database [33] obtained from various LWR fuels; one group subjected to no power ramps during normal operation and the other one experienced power ramping at the end of its life. Table 1 shows that the database for normal operation covers both the manufacturing parameters and operating conditions for LWR fuels; the average rod burnup of 13.0–52.7 MWd/kgU, average linear power of 92–300 W/cm, fuel density of 93.9–95.3% of theoretical one, fill gas pressure of 6.5–27.5 atm, and grain size of 8–10 μm. Table 2, which covers the database for power ramped fuels, shows the burnup, initial power just prior to ramp, maximum terminal power, ramp rate, and holding time at maximum terminal power. Fig. 2 indicates that the present model is in reasonable agreement with the measured data, where, the average ratio of calculated to measured data is 1.24.

Gas release at BWR rods during post-irradiation annealing [31] shown in Fig. 3 was analyzed using the following procedure. First, gas disposition among the matrix, grain face and grain edge at the end of base irradiation, calculated with 0.50 for f_b^{max} and 0.07 for $(\Delta V/V)_e^{max}$, was used as the initial condition for the subsequent analysis for post-irradiation annealing. Second, gas release during the temperature ramp, which is different from the power ramp given in Section 2.5.4, was calculated using the assumption that once the threshold temperature for burst release observed in the experiment was reached, all the gases retained on the grain face and at grain edge are released immediately. The observed threshold temperatures for the burst

Table 1
Fission gas release data obtained from LWR fuels subjected to no power ramps during irradiation

	Burnup (MWd/kgU)	Average linear power (W/cm)	Fuel density (% TD)	Fill gas He pressure (bar)	Grain size (μm)	Measured release (%)
Reactor A	23.2	94–269	95.1	6.5	8	17.2
	23.1	100–280	95.1	6.5	8	14.8
	22.7	130–278	95.3	6.5	8	7.2
Reactor B	13.0	176–241	93.9	22.5	10	0.9
	13.3	182–249	93.9	22.5[a]	10	24.8
	26.5	178–289	93.9	22.5	10	3.9
	26.2	185–291	93.9	22.5[a]	10	17.8
	36.9	166–298	93.9	22.5	10	3.7
	36.5	173–300	93.9	22.5[a]	10	16.5
	33.0	92–254	95.3	6.5	8	11.8
	36.5	140–270	95.3	6.5	8	3.6
Reactor C	43.5	170–232	95.3	27.5	10	1.2
	23.1	100–280	95.1	6.5	10	1.9
	14.4	222–272	95.0	22.5	10	0.6
	29.0	263–288	94.3	22.5	10	4.5
	40.8	219–297	94.3	22.5	10	3.3
	47.2	180–262	94.3	22.5	10	2.6
	52.7	160–270	94.3	22.5	10	2.1

[a] In these cases, Ar is filled instead of He.

Table 2
Fission gas release data obtained from LWR fuels subjected to a power ramp at the end of life

	Burnup (MWd/kgU)	Power before ramp (W/cm)	Maximum terminal power (MTP) (W/cm)	Ramp rate (W/cm min)	Holding time at MTP (h)	Grain size (μm)	Measured release (%)
Reactor D	26.7	290	400	100	52	8	25.7
	25.7	290	370	100	52	8	4.6
	21.7	290	435	100	1	6	6.3
	22.8	290	420	90	8	10	11.7
	24.2	280	445	95	53	10	37.5
	43.2	245	350	90	0.5	6	16.0
	44.5	245	417	90	0.5	10	20.1
Reactor E	34.7	250	415	90	12	10	8.5
	34.4	250	475	90	12	10	22.1
	44.0	250	410	85	12	10	28.0
	43.4	250	490	85	12	10	44.9
	24.3	300	445	85	24	10	3.0
	32.3	190	419	85	195	10	48.3
Reactor F	20.3	296	405	–	48	8	16.2
	20.9	296	405	–	–	8	2.3

release were 1800°C for the 6 MWd/kgU specimen, 1600°C for the 16 MWd/kgU specimen and 1500°C for the 23 and 28 MWd/kgU specimens, respectively [31].

Finally, to calculate gas release during annealing period at 1800°C, f_b^{max} and $(\Delta V/V)_e^{max}$ are assumed to increase linearly with time from their respective value of zero just after the burst release up to their maximum value of 0.25 and 0.05 when a certain time, which is given in the following, elapses at the annealing temperature of 1800°C. This assumption implies that, once the gas atoms on the grain boundaries are purged by burst release due to the rapid interconnection of intergranular bubbles and the formation of release tunnels [31,34], the number of gas atoms needed to fill the grain boundaries is almost zero just after the burst release because of the already well-established release tunnels. Then during the

annealing period, these tunnels might be destroyed and hence the number of gas atoms required on the grain face and at grain edge to re-establish release pathways would increase. External restraint stress in this test was considered to be zero [3]. The maximum values of 0.25 and 0.05 for f_b^{max} and $(\Delta V/V)_e^{max}$ during the annealing period, which are lower than those for the steady-state values of 0.50 and 0.07, were chosen because they yielded more reasonable calculation results.

According to the calculations made for 4 cases without changing the model parameters, that is, by using the constants of 0.25 and 0.05 for f_b^{max} and $(\Delta V/V)_e^{max}$ throughout the annealing experiment, it took about 2 and 4 h for f_b^{max} and $(\Delta V/V)_e^{max}$ to reach their respective maximum values. This suggests that the average time required for the complete establishment of release path at the grain boundaries is about 3 h. This fact corresponds to the assumption that, if f_b^{max} and $(\Delta V/V)_e^{max}$ increase linearly from zero with time after the burst release, it would take 6 h until f_b^{max} and $(\Delta V/V)_e^{max}$ reach their maximum values of 0.25 and 0.05. Therefore, it is assumed for all four specimens that f_b^{max} and $(\Delta V/V)_e^{max}$ would reach their maximum values when 6 h has been spent at the annealing temperature of 1800°C after the gas inventory accumulated at grain boundaries during base irradiation is purged by burst release at the threshold temperature of 1500–1800°C.

For the specimen of 6 MWd/kgU, the calculated gas release after base irradiation was 0.11%, while the measured one was 0.2%. As shown in Fig. 3(a), the burst release of about 2.5% is predicted to occur and then the calculated release remains almost constant for about 1 h until additional gas atoms reach the grain boundaries. While the calculated burst release is assumed to take place instantaneously, the measured burst release of 4.5% occurred for about 30 min during the experiment [31]. This partly explains why there exists discrepancy between the calculated and measured releases at the early stage of the annealing experiment where burst release occurs. Another source of the discrepancy would result from the fact that the external restraint stress on grain boundary bubbles, which was assumed to be zero [3], could have been greater than zero and hence the grain boundary bubbles would have existed as non-equilibrium bubbles [31]. Then, for the same values of f_b^{max} and $(\Delta V/V)_e^{max}$, more gas atoms might have been retained on the grain boundary bubbles during the base irradiation and this could have led to more calculated burst release thereby reducing the difference between the calculated and measured values.

The calculated and measured releases were 0.8% and 0.5%, respectively, for the specimen of 16 MWd/kgU taken from the fuel pellet irradiated for 2 cycles. Fig. 3(b) shows that, when the specimen temperature reached

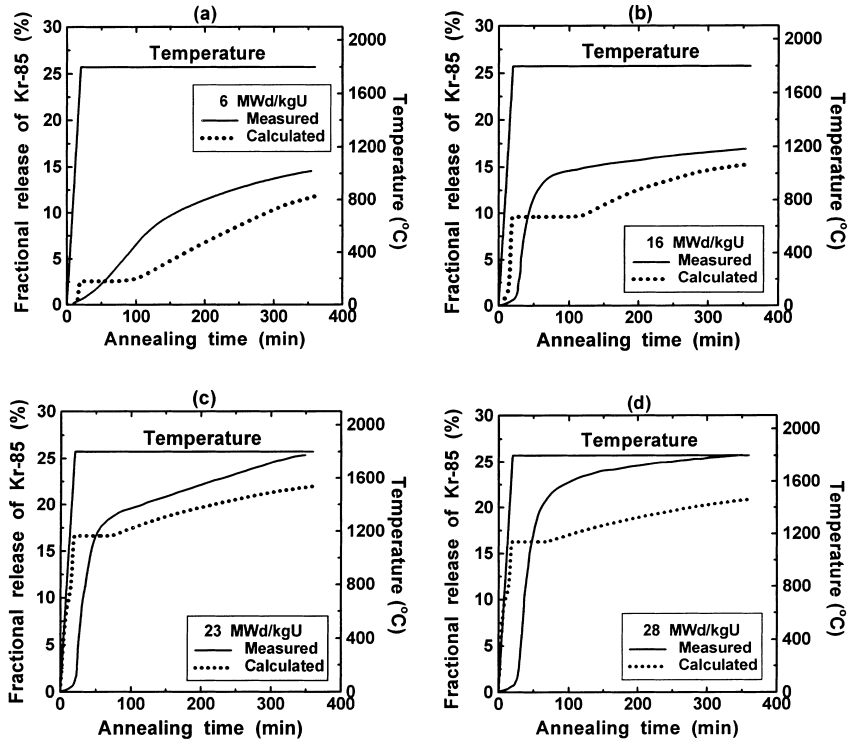

Fig. 3. Fractional release of Kr-85 during temperature ramp and isothermal annealing at 1800°C [31].

1600°C, the model predicted that almost all gas atoms retained at grain boundaries are released and then no release occurs until additional gas atoms arrive at the grain boundaries by diffusion. The difference in release kinetics between the measurement and calculation can be explained by the same argument given for the specimen of 6 MWd/kgU, that is, while the measured burst release lasted for about 30 min [31] after the threshold temperature was reached, the calculation assumes instantaneous release when fuel temperature reaches the threshold one.

For the specimens of 23 and 28 MWd/kgU obtained from the pellets irradiated for 3 and 4 cycles, gas releases after base irradiation were both 21%, respectively [31], which were unusually high for fuel with this range of burnup. Analysis of gas release for the fuel that was refabricated from pre-irradiated one should be performed after the calculated release for the pre-irradiated fuel is fitted to the measured one. Therefore, b_f was reduced from 10^{-5} to 10^{-6} while the values for f_b^{max} and $(\Delta V/V)_e^{max}$ remained unchanged. This reduction in b_f yielded 18.5% and 24.8% releases after base irradiations for the 3 and 4 cycle-irradiated fuels. Fig. 3(c) and (d) show that, though the burst releases are underpredicted, diffusional releases during 1800°C are well predicted, suggesting that the gas inventory retained at the grain boundaries was likely to be underpredicted for the base irradiated fuels.

Fig. 4 displays a parametric study which shows that external restraint stress has a significant effect on gas release at 1400°C. At a constant temperature, the establishment of release tunnels by grain edge bubbles, which is governed by gaseous swelling, is delayed as the external restraint stress increases because more gas atoms can be retained on the grain boundaries as indicated by Eqs. (11) and (18). Therefore, from the viewpoint of current trend to extend discharge burnup, an improved understanding of the role of external stress on gas release at high burnup fuel, where very large external stress can occur by PCMI and high rod internal pressure, is indispensable.

Zimmermann [1] carried out an isothermal irradiation of UO_2 fuel to investigate the gas release and swelling under both with and without external restraint. Fig. 5 shows that, while some discrepancies exist at low burnup between the calculation and measurement for 1750 and 2000 K, the agreement is very good for 1250 and 1500 K under unrestrained conditions.

Fig. 6 compares the gaseous swelling under restrained conditions as a function of burnup for different irradiation temperatures. The calculations for the data whose pressures during the experiment had been 25–50 MPa [1] were made using the parameters of 0.50 and 0.07 for f_b^{max} and $(\Delta V/V)_e^{max}$. External stress on fuel pellets for these data was taken to be 37 MPa, the mean value of 25 and 50 MPa. The calculated gaseous swelling, which is the sum of the maximum swelling of 7% induced by grain edge bubbles and 1% or 2% swelling by grain face bubbles, ranges from 8.5% to 10% depending on irradiation temperature. The measured gaseous swelling was obtained by taking into account a solid swelling rate of about 0.65% per percentage burnup in-

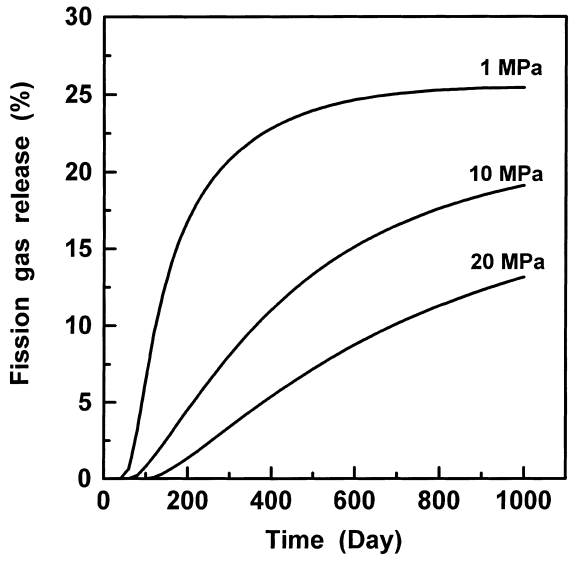

Fig. 4. Calculated fission gas release as a function of external restraint stress at the fuel temperature of 1400°C.

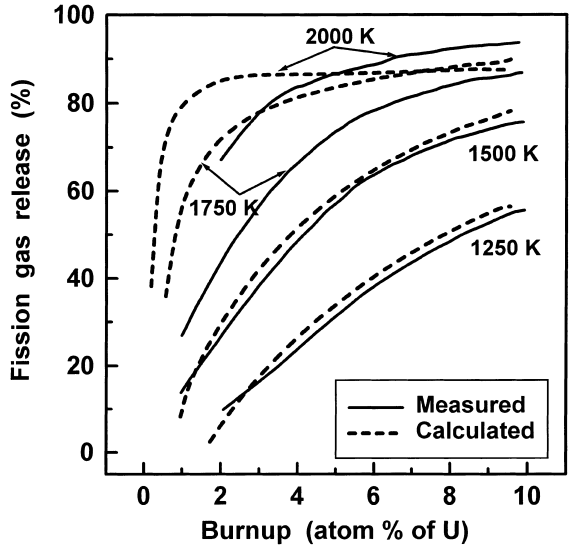

Fig. 5. Fission gas release from UO_2 specimen as a function of isothermal irradiation temperature under unrestrained conditions [1].

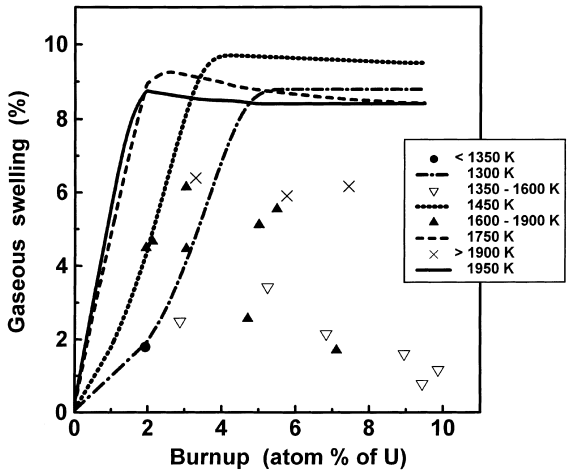

Fig. 6. Swelling of UO_2 specimen as a function of isothermal irradiation temperature under restrained conditions (lines: calculated; symbols: measured) [1].

duced by solid fission products. The calculated maximum swelling of 8.5–10% is consistent with Kashibe and Une's [7] result that the saturated swelling, though obtained from an experiment for unirradiated fuel, was 8–10% for the external restraint stresses of 37 MPa at 1450°C and 73 MPa at 1350°C.

However, the measured gaseous swelling shows two different trends. Although some scattering exists in the data, the measured swelling corresponding to fuel temperatures above 1600 K is saturated at about 6% for burnup larger than 3 at.%. This value can be understood as the gaseous swelling at which release path is fully established and therefore additional gas atoms reaching the grain boundaries had been released without inducing any further swelling. Considering 1–2% contribution from the grain face bubbles, the gaseous swelling caused by the grain edge bubbles appears to be around 5%, which is close to the value given in [17]. For fuel temperatures between 1350 and 1600 K, the measured gaseous swelling decreased down to 1% after it reached around 3.5% at 5% burnup. This is not consistent with the assumption used in this study that, once the grain edge tunnels are developed with gas bubbles, they would be stable for constant fuel temperature. Decrease in gaseous swelling could arise if some fraction of gas atoms forming the release path would be vented together with the additional gas atoms arriving at grain edges. For fuel temperatures below 1350 K, since only one data is available, it is difficult to make any comparison.

The gas release data obtained from the Risϕ-III Project [35,36] were also used to verify the present model. Of the all power ramping tests performed on the ANF fuel (PWR) and GE fuel (BWR) in the DR3 reactor at Risϕ, 3 tests of AN3, AN4, and AN10 for PWR fuel and another 3 tests of GE2, GE4, and GE6 for BWR fuel were analyzed. All of these 6 tests were performed with a thermocouple and a pressure transducer equipped so that fuel centerline temperature and rod internal pressure could be measured during test irradiation. The external restraint stresses on fuel pellets were taken to be 27 MPa for AN3 and AN4 and 23 MPa for AN10 [3]. For GE fuel, they were 50, 6 and 17 MPa for GE2, GE4 and GE6, respectively. Since the analyses results for the ANF and GE fuel show almost the same trend, only the two cases of the AN3 for ANF fuel and the GE6 for GE fuel are described.

The AN3 fuel had been base-irradiated in the Biblis-A reactor in Germany to about 44 MWd/kgU. The highest linear power experienced by this fuel was 26.7 kW/m and gas release during base irradiation did not exceed 0.3%. The transient test for the fuel was carried out in the DR3 reactor at Risϕ. The maximum power reached during the test was 40.7 kW/m [35]. Fig. 7(a) compares the calculated and measured centerline temperature obtained during the transient test. It is to be noted that the measured centerline temperature shown here and also that for the GE6 fuel in Fig. 8(a) was obtained by converting the measured temperature for

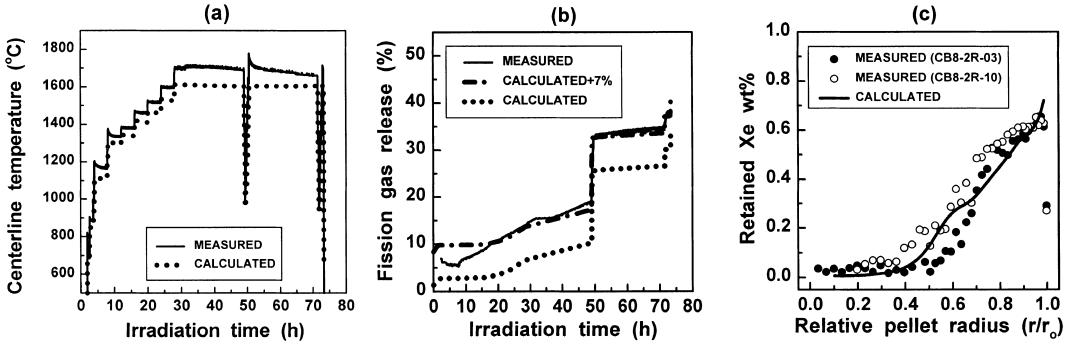

Fig. 7. Analysis results for the Risϕ-III AN3 test: (a) centerline temperature; (b) fission gas release; (c) radial distribution of Xe [36].

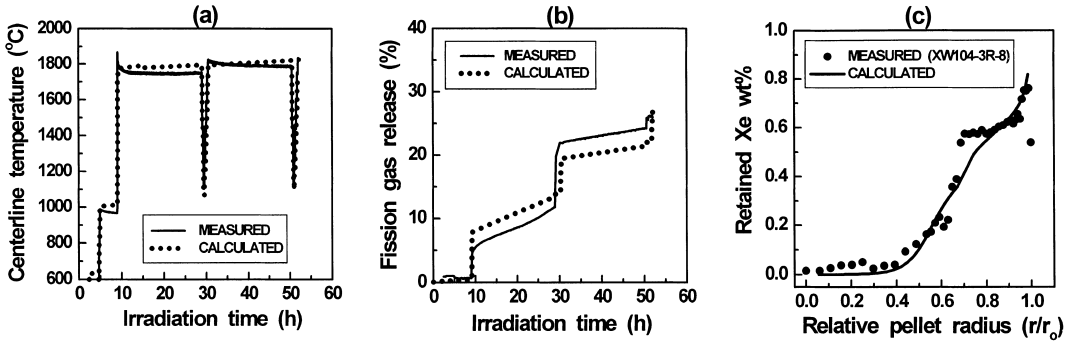

Fig. 8. Analysis results for the Risϕ-III GE6 test: (a) centerline temperature; (b) fission gas release; (c) radial distribution of Xe [36].

annular pellets into the one corresponding to solid pellets [35]. Temperature distribution across the fuel pellet was calculated considering the effect of conductivity degradation with burnup and rim formation at pellet periphery [37]. The maximum difference between the calculated and measured centerline temperature was around 100°C.

To calculate the transient gas release for the Risϕ-III Project, it was assumed that all gas atoms on the grain faces and at grain edges are released instantaneously if the change in linear power during power ramp was larger than 30–40 W/cm and the linear power just prior to power excursion was above 310–400 W/cm depending on the cases analyzed. These values, which are larger than those given in Section 2.5.4, were selected because they yielded more reasonable results when power ramp occurred. This fact indicates that the model constants for transient gas release should be determined from a large number of data, that is, on a statistical basis. In addition, after the condition for burst release was satisfied, based on the following argument, f_b^{max} and $(\Delta V/V)_e^{max}$ were assumed to vary by the same way as used for Fig. 3; microcracks created by thermal stress would be healed progressively during the high power (temperature) period leading to increase in f_b^{max} and $(\Delta V/V)_e^{max}$ from zero to their original values of 0.25 and 0.05, respectively. This means that as the microcracks are healed, the number of gas atoms needed for the completion of release tunnels increases. The time required for the full recovery of f_b^{max} and $(\Delta V/V)_e^{max}$ was taken to be 40 h for the AN3 fuel, because this was the difference between the time when the conditions for burst release were first satisfied and the one when the second burst release took place just after the high power period (see Fig. 7(b)). It is very probable that the diffusion of matrix material needed for the healing of microcracks might have occurred during this high power period.

Fig. 7(b) shows that the calculated gas release is lower than the measured one. However, according to Mogensen et al. [38], there were some athermal gas releases of 6–7% during the tests at a low power of 11 kW/m due to the peculiar fabrication characteristics specific to the AN3, AN4 and AN10 fuel. This rather high athermal gas release, which is an unusual phenomenon that is not found in typical fuel, was observed in the low density fuels where fission gases might have been collected in the fabrication pores during steady-state irradiation and then released during power ramps through cracks. Therefore, when 6–7% was added to the calculated value, very good agreement was obtained. The linear power of 300–400 W/cm just prior to power excursion for burst release is consistent with the experiments showing that the onset of gas release for the Risϕ-III type fuel was found at power levels between 300 and 370 W/cm [39].

Fig. 7(c) shows the radial distribution of residual Xe atoms measured by EPMA in fuel pellets after the ramp test in terms of a fractional weight relative to that of UO_2. Measurement clearly indicates that, when the fuel was maintained at a centerline temperature of around 1800°C for 20 h, the fission gas atoms in the matrix and at the grain boundaries were almost exhausted by release up to the relative pellet radius of about 0.4–0.5. Since EPMA measures the Xe atoms dissolved in fuel lattice and trapped in intragranular bubbles smaller than about 0.1 μm, only the Xe atoms in the grain interior were considered in the calculation.

GE6 fuel had been base-irradiated in the Millstone-1 reactor in the USA to about 45 MWd/kgU. The highest linear power of this fuel was 32.1 kW/m and gas release during base irradiation was below 0.3%. The transient test for this fuel was also performed in the DR3 reactor at Risϕ. The maximum power achieved during the test was 37.9 kW/m [35]. Fig. 8 displays the measured and calculated centerline temperature, gas release and retained Xe. Since the measured temperature after the irradiation time of 53 h was considered unreliable [36], analysis was made only up to this point. As for the ANF fuel, the maximum deviation of centerline temperatures

for GE fuel was around 100°C. Gas release, which did not have athermal contribution in contrast with the ANF fuel [38], and the radial distribution of retained Xe were well simulated.

4. Conclusions

A model, which considers the effect of PCMI and high internal pressure encountered at high burnup, has been developed to analyze fission gas release and gaseous swelling in UO_2 fuel. Using the assumption that a UO_2 grain surface consists of 14 identical circular faces and a grain edge bubble can be represented by a triangulated tube around the circumference of three circular grain faces, the model is focused on the behavior of grain boundary bubbles considering the effect of external restraint. Furthermore, it introduces the concept of formation of release tunnels that is proportional to the gas bubble swelling at grain edge. Main model parameters are the maximum fraction of grain face covered by gas bubbles f_b^{max}, the maximum swelling by grain edge bubbles $(\Delta V/V)_e^{max}$ when the release path is fully established, and the external stress. The following conclusions are drawn from the analyses of the measured data obtained from a wide range of operating conditions:

1. The model parameters of 0.50 and 0.07 for f_b^{max} and $(\Delta V/V)_e^{max}$ provide a good prediction of gas release for the data obtained from LWR fuel that experienced steady-state and/or transient operation.
2. The external restraint stress has a significant effect on the gaseous swelling of grain face and grain edge bubbles and thereby affects the formation of release paths both at the grain face and grain edge through f_b^{max} and $(\Delta V/V)_e^{max}$.
3. The requirement for burst release during power ramp should be obtained on a statistical basis due to uncertainty related to the creation of microcracks by change in thermal stress. For example, the threshold linear power just prior to power ramp and the change in power during the ramp was 250 and 30 W/cm, respectively, for the database obtained from various LWR fuels. On the other hand, the threshold linear power ranged from 310 to 400 W/cm and the change in power during the ramp was 30–40 W/cm for the fuel rods tested in the Risϕ-III Project.
4. The fact that the use of 0.25 and 0.05 rather than 0.50 and 0.07 for f_b^{max} and $(\Delta V/V)_e^{max}$ yields more reasonable agreement with measured data for both temperature and power ramp implies that the grain boundary's ability to retain gas atoms is reduced once the gas atoms in the grain boundary are purged via rapid temperature rise or power ramp.
5. Combined with the characteristics of a fuel performance analysis code COSMOS, the present model has been able to analyze the data obtained from refabricated fuel segments or post-irradiation annealing experiments.

Acknowledgements

The authors would like to express their appreciation to the Ministry of Science and Technology (MOST) of the Republic of Korea for the support of this work through the mid- and long-term nuclear R&D Project. In addition, the authors would like to thank Dr T. Kogai of Toshiba Corporation for his valuable suggestions in data preparation for typical BWR fuels.

References

[1] H. Zimmermann, J. Nucl. Mater. 75 (1978) 154.
[2] T. Kogai, K. Ito, Y. Iwano, J. Nucl. Mater. 158 (1988) 64.
[3] T. Kogai, J. Nucl. Mater. 244 (1997) 131.
[4] C.T. Walker, P. Knappik, M. Mogensen, J. Nucl. Mater. 160 (1988) 10.
[5] J.A. Turnbull, M.O. Tucker, Philos. Mag. 30 (1974) 47.
[6] M.O. Tucker, Radiat. Eff. 53 (1980) 251.
[7] S. Kashibe, K. Une, J. Nucl. Mater. 247 (1997) 138.
[8] M.O. Tucker, J. Nucl. Mater. 79 (1979) 199.
[9] Y.H. Koo, B.H. Lee, D.S. Sohn, J. Korean Nucl. Soc. 30 (1998) 541.
[10] J. Weisman, P.E. Macdonald, A. Miller, H.M. Ferrari, ANS Trans. 12 (1969) 900.
[11] C. Baker, J. Nucl. Mater. 71 (1977) 117.
[12] M.H. Wood, J.R. Matthews, J. Nucl. Mater. 91 (1980) 35.
[13] R.J. White, M.O. Tucker, J. Nucl. Mater. 118 (1983) 1.
[14] J.A. Turnbull, C.A. Friskney, J.R. Findlay, F.A. Johnson, A.J. Walter, J. Nucl. Mater. 107 (1982) 168.
[15] J.R. Matthews, M.H. Wood, J. Nucl. Mater. 91 (1980) 241.
[16] M.R. Hayns, M.H. Wood, J. Nucl. Mater. 59 (1976) 293.
[17] M.O. Tucker, J.A. Turnbull, Proc. Roy. Soc. 343 (1975) 229.
[18] J.A. Turnbull, J. Nucl. Mater. 50 (1974) 62.
[19] W. Beere, G.L. Reynolds, J. Nucl. Mater. 47 (1973) 51.
[20] G.E. Pile, Seager, Phys. Rev. B 10 (1974) 1421.
[21] P. Knudsen, C. Bagger, H. Carlsen, I. Misfeldt, M. Mogensen, Nucl. Tech. 72 (1986) 258.
[22] M. Mogensen, C.T. Walker, I.L.F. Ray, M. Coquerelle, J. Nucl. Mater. 131 (1985) 162.
[23] F. Sontheimer, P. Dewes, R. Manzel, H. Stehle, IAEA Technical Committee Meeting on Fuel Rod Internal Chemistry and Fission Product Behavior, Karlsruhe, 1985.
[24] M.J.F. Notley, I.J. Hastings, J. Nucl. Mater. 56 (1980) 163.
[25] B.J. Lewis, J. Nucl. Mater. 148 (1987) 28.
[26] D.R. Olander, Fundamental Aspects of Nuclear Reactor Fuel Elements, TID-26711-P1 (1976).
[27] M. Oguma, Nucl. Eng. Des. 76 (1983) 35.
[28] J.C. Wood, B.A. Surette, I. Aitchison, W.R. Clendening, J. Nucl. Mater. 88 (1980) 81.

[29] W. Hering, Description of the new mechanistic fission gas release model, KWU, 1989.
[30] E. Porrot, F. Lefebvre, M. Charles, C. Lemaignan, in: Proceedings of the International Topical Meeting on LWR Fuel Performance, Williamsburg, VA, USA, 17–20 April 1988, p. 267.
[31] K. Une, S. Kashibe, J. Nucl. Sci. Tech. 27 (1990) 1002.
[32] D. Dowling, R. White, M. Tucker, J. Nucl. Mater. 110 (1982) 37.
[33] Y.H. Koo, B.H. Lee, D.S. Sohn, KAERI's Fuel Performance Database, 1990 (unpublished work).
[34] I. Zacharie, S. Lamsiart, P. Combette, M. Trotabas, M. Coster, M. Groos, J. Nucl. Mater. 255 (1998) 85.
[35] C. Bagger, M. Mogensen, C.T. Walker, J. Nucl. Mater. 211 (1994) 11.
[36] P.M. Chantoin, E. Sartori, J.A. Turnbull, The Compilation of a Public Domain Database on Nuclear Fuel Performance for the Purpose of Code Development and Validation, OECE/NEA, Paris, 1997.
[37] B.H. Lee, Y.H. Koo, D.S. Sohn, in: Proceedings of the IAEA Technical Committee Meeting on Advances in Pellet Technology for Improved Performance at High Burnup, Tokyo, October 28–November 1 1996, p. 205.
[38] M. Mogensen, C. Bagger, H. Toftegaard, P. Knudsen, C.T. Walker, J. Nucl. Mater. 202 (1993) 199.
[39] P. Knudsen, C. Bagger, H. Carlsen, B.S. Johansen, M. Mogensen, I. Misfeldt, in: Proceedings of the International Topical Meeting on LWR Fuel Performance, Williamsburg, VA, USA, 17–20 April 1988, p. 189.